Article

Identifying Organic Matter (OM) Types and Characterizing OM Pores in the Wufeng−Longmaxi Shales

Guoliang Xie* and Weiduo Hao

Read Online

ACCESS | Metrics & More | Article Recommendations

ABSTRACT: Organic matter (OM) pores are considered to be an important pore type in the Ordovician Wufeng−Silurian Longmaxi Formation shales in the Sichuan Basin, China, because they have a high capacity to store natural gas. However, to the best of our knowledge, research on the characterization and quantitation of different OM pore characteristics is insufficient. In this study, detailed optical microscope and scanning electron microscope (SEM) observations and the pores/particles and cracks analysis system (PCAS) were applied to identify the OM pores and obtain quantitative information on pores such as pore size, surface porosity, form factor, and probability entropy. Moreover, CO_2 and N_2 adsorption experiments were performed to study the properties of pores for samples with different TOC and mineral compositions. The results show the following. (1) Pyrobitumen and kerogen can be distinguished under an optical microscope and SEM; the former can be further divided into pyrobitumen without a fixed shape and pyrobitumen with a certain shape, and the latter contains algal fragments, bacteria-like aggregates, graptolite, and micrinite. The overwhelming number of SEM-visible OM pores are mainly observed in pyrobitumen without a fixed shape, whereas pores in other OM types are complex. A PCAS analysis showed that meso-macropores are developed in pyrobitumen without a fixed shape, whereas pores in algal fragments and bacterial-like aggregates are mainly mesopores. (2) Quartz-rich brittle shale will provide more visible SEM pores compared to clay-rich ductile shale, and carbonates are unfavorable for pore development because they can block the pore as cements. Moreover, the rigid mineral framework, including that constructed by quartz recrystallization and pyrite cementation, and the pore-fluid pressure are favorable for the development of OM pores. (3) Adsorption experiments showed that pyrobitumen makes a great contribution to pore development, including micropores and meso-/macropores. Finally, we propose that the pore parameters (e.g., pore diameter, pore form factor, and deformation) of pyrobitumen without a fixed shape may characterize the enrichment condition of shale gas.
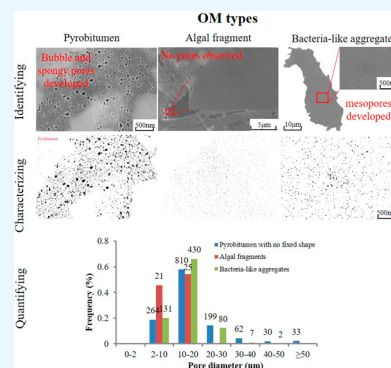
1. INTRODUCTION

Shale gas is a clean and efficient unconventional natural gas resource, which has attracted extensive attention in China.[1−3] As a gas reservoir, shale is characterized by low porosity and ultralow permeability due to its micro-/nanopore structures.[4,5] Organic matter (OM) pores in shales are believed to store most of the shale gas in a shale formation due to the facts that (1) OM pores have higher porosity compared to other pore types and provide more pore spaces for gas storage[5] and (2) they show a higher adsorption capacity for gases and can provide abundant binding sites.[6] Therefore, OM pores have received extensive attention in recent years.

The Wufeng−Longmaxi shale is one of the largest reservoirs for shale gas exploration and development in China, which is mainly developed in the Sichuan Basin. The shale gas production in the Sichuan Basin was already above 230×10^8 m^3 by the end of 2021. Numerous studies have been conducted on the Wufeng−Longmaxi shales from the aspects of depositional conditions,[7,8] physical properties,[9,10] shale gas accumulation,[10−13] and pore structure characteristics.[14−17] In

terms of OM pore structure, great attention have been given;[17−26] however, some key issues remain unresolved.[17,27,28]

First, the identification of the types of OM is still contentious. Some researchers reported that primary kerogen macerals such as algae and alginite are dominant in the Wufeng−Longmaxi shale,[29] whereas others suggested that the secondary solid bitumen is dominant.[30,31] For example, Chen et al.[32] divided the OM of Wufeng−Longmaxi shale into shaped OM and amorphous OM based on whether the OM has a regular shape. The shaped OM is mainly graptolite, while amorphous OM is mostly composed of bitumen and micrinite. Yang et al.[33] suggested that OM in Wufeng−Longmaxi shale is predominately pyrobitumen, followed by graptolite and
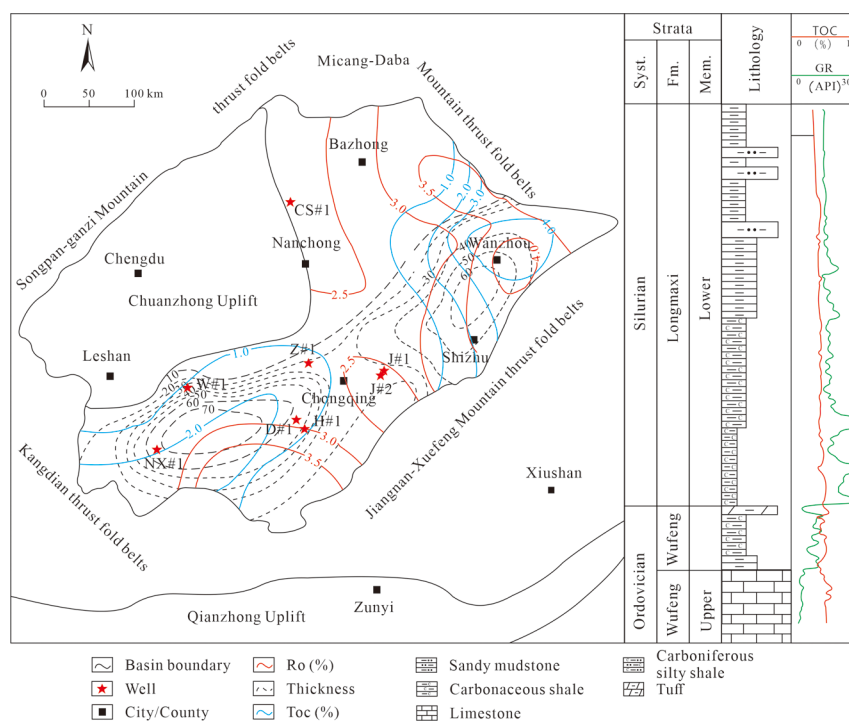
Figure 1. Location of shale samples and vertical profiles of the Wufeng−Longmaxi shale.

Table 1. TOC Content, Vitrinite Reflectance (ER$_o$), and Mineral Composition of Samples

well	sample	depth (m)	TOC (%)	ER$_o$ (%)	mineral composition (%)				clay minerals (%)			
					quartz	feldspar	carbonate	pyrite	clay	illite	chlorite	illite/smectite mixed layer
CS#1	C1-1	7137	2.32		44	5	21	3	23			
	C1-2	7143	4.2	2.09	71	3	12	2	5			
	C1-3	7149	4.36	2.14	75	2	11	2	7			
Z#1	Z1-1	3866.9	0.97		40	5	0	3	52			
	Z1-2	3877.09	2.25	2.2	35	9	17	2	37			
	Z1-3	3887.76	2.36	2.37	48	12	13	2	25	73	23	4
	Z1-4	3891.72	4.40	2.45	68	4	5	5	18	78	17	5
	Z1-5	3897.4	3.71	2.33	67	5	3	6	19	80	15	5
NX#1	N1-1	3933.75	3.16	2.67	33	1	63	1	2			
	N1-2	3934.17	4.4	2.62	68	3	9	3	5	79	18	3
	N1-3	3944.4	1.82	2.73	44	2	36	2	8	65	31	4
H#1	H1-1	4114	3.27	2.64	53.5	7.7	6.6	4.1	28.1			
	H1-2	4127.6	2.05	2.70	34	5.7	26.9	1.5	31.9			
W#1	W1-1	2549.5	2.65	2.12	35	5	31	1	28	74	20	6
	W1-2	2577	2.69	2.16	31	0	65	2	2			
J#1	J1-1	2570	2.48	3.0	56	7	8	3	32			
J#2	J2-1	2586	4.58		46.5	12	5.5	2	24			
D#1	D1-1	3695.76	2.93	2.87	42	3	38	5	12	82	9	9

micrinite. Most likely, the difficulty in identifying OM types and related OM pores may be attributed to the lack of appropriate methods and samples. In addition, controversy remains with regard to the development and distribution of OM pores. For instance, some researchers pointed out that nearly no pores are observed in graptolites for Wufeng− Longmaxi shale,[27] whereas others suggested that graptolites contain abundant OM pores.[32]

Second, there is very limited research on a quantitative characterization of OM pores.[27,33] In general, SEM observations can only probe into pores with a pore diameter larger than 5 nm.[4,34] However, there are significant numbers of

studies which revealed that OM pores that are smaller than 5 nm are abundant. Therefore, more techniques such as gas adsorption experiments should be applied to investigate small pores in order to have a better understanding of porosity and permeability in shales.

In this study, our objective is to comprehensively investigate OM types and quantitatively characterize the typical OM pores in Wufeng−Longmaxi shale. The ultimate idea is to have a better understanding of the pore information, which can then be used to indicate gas storage in the Sichuan Basin.

2. GEOLOGICAL SETTING

The Sichuan basin is situated at the northwest margin of the Yangtze Platform with an area of 18×10^4 km^2, which is surrounded by the Micangshan−Dabashan thrust fold belts, Jiangnan−Xuefengshan thrust fold belts, Kangdian thrust fold belts, and Songpan−Ganzi fold belts (Figure 1). During the period from the late Ordovician to early Silurian, the Sichuan Basin was affected by the force of Caledonian movement and several uplifts such as a Chuanzhong uplift, Qianzhong uplift, and Jiangnan−Xuefeng uplift were formed.[35] During this period, relatively low energy and anoxic conditions were dominant in the southeast Sichuan Basin with the rise of sea level, which resulted in the deposition of thick, organic-rich Wufeng−Longmaxi shale in this region.[36,37] The Wufeng−Longmaxi shale is located between the Upper Ordovician Wufeng Formation and the Lower Silurian Longmaxi Formation, which was deposited in deep-water shelf environment with a thickness ranging from 10 m to over 70 m[38] (Figure 1). The Wufeng−Longmaxi shale in the southeast Sichuan Basin is mainly composed of black carbonaceous and siliceous shale with abundance graptolites such as *Amplexograptus, Diceratograptus, Dicellograptus, Tangyagraptus*, etc.[37] Note that the Wufeng−Longmaxi shale belongs to a set of shales distributed all over the world in the Silurian period. The early Silurian shale is called "hot shale" in North Africa and the Middle East, which is characterized by high TOC content, high γ-ray (GR) value, and abundant graptolites.[39]

3. SAMPLES AND EXPERIMENTS

3.1. Samples. A total of 18 samples from the Wufeng−Longmaxi Formation were collected from eight wells in the Sichuan Basin (Figure 1). Detailed information on these samples is given in Table 1. Note that our samples selected are all overmature, with ER$_o$ values ranging from 2.0% to 3.0%, and the reason for selecting these samples for this study is to determine the relationship between OM maturity and the OM pore development in the Wufeng−Longmaxi shale.[40]

3.2. Experiments. *3.2.1. OM Geochemistry and Mineral Composition Analysis.* The geochemistry of OM and the mineral composition were analyzed at the Keyuan Engineering Technology Testing Center of Sichuan Province, China. TOC analysis was performed by using a LECO C230 Elemental Analyzer according to the standard GB/T19145-2003, whereas OM maturity of shale was obtained by testing the bitumen reflectance using a MPV-3 microphotometer according to the standard SY/T 5124-2012. Since the Wufeng−Longmaxi shale has no input of terrestrial organisms (vitrinite), the solid bitumen/pyrobitumen reflectance (BR$_o$) can be converted to the equivalent vitrinite reflectance (ER$_o$) using the formula ER$_o$ = 0.4 + 0.618 × BR$_o$.[41] The mineral composition was determined by using a D8 Advance X-ray diffractometer.

3.2.2. Field Emission Scanning Electron Microscopy (FE-SEM). FE-SEM analyses were conducted on 15 samples. Each sample was cut to a size of $8 \times 8 \times 3$ mm^3 and wet-polished with ultrathin emery paper with sizes of 30, 15, 9, 6, 3, and 1 μm in sequence in order to reduce the surface roughness for better argon ion milling. The purpose of this step was to ensure that the surface of the samples is parallel to the bedding. FE-SEM analysis was conducted using a Hitachi su8220 scanning electron microscope equipped with a second electron detector and a backscattered electron detector at the South China University of Technology, Guangzhou, China. Before observation of the areas of interest, the surface of the samples needs to be coated with a layer of platinum to improve conductivity. A total of 80−100 SEM images for each sample were captured at magnifications of ×10k, ×25k, ×50k, and ×100k.

3.2.3. N$_2$ and CO$_2$ adsorption. A combination of N$_2$ and CO$_2$ adsorption experiments was performed to investigate the pore size distribution. In theory, N$_2$ adsorption is applied to characterize meso-/macropores, whereas CO$_2$ adsorption is suitable for the characterization of micropores.[42−44]

A low-pressure N$_2$ adsorption experiment was conducted using a Quadrasorb SI Automated Surface Area & Pore Size Analyzer in the State Key Laboratory of Oil and Gas Reservoir Geology and Exploitation, Chengdu University of Technology. One to two grams of samples of 60−80 mesh size were weighed and then outgassed by a Flovac Degasser at 110 °C for over 12 h to remove the bound water in shale. The adsorption−desorption isotherm curves were obtained at relative pressures (P/P_0) ranging from 0.01 to 0.995. In this study, the quenched solid density functional theory (QSDFT) model was used to provide information on pore size ranging from approximately 0.9 to 30 nm.[26]

CO$_2$ adsorption was conducted at relative pressures (P/P_0) ranging from 0.0004 to 0.032 at 273 K using an ASAP 2000 HD88 Analyzer at the Beijing Center for Physical & Chemical Analysis. The DFT model was applied to provide the information on pore sizes ranging from 0.3 to 1.4 nm.

3.3. PCAS Image Processing Method. To quantitatively characterize the parameters of pore structure, including pore size, pore surface porosity, and pore morphology, PCAS was applied to process SEM images. First and foremost, selecting an appropriate threshold is the key when using PCAS to process SEM images. Our principle is to adjust the threshold so that the pores are completely filled. It is noted that the resolution of SEM images is about 5 nm; thus the pores less than 5 nm are not seen. The related definition and explanation of geometric parameters in PCAS have been given by Liu et al.[45] and Jiao et al.[26,46] Among these parameters, the form factor can indicate the regularity of pores, a form factor of 1.0 represents a perfect circle, whereas a form factor of 0.75 represents a square in 2D images. An increase in the form factor can decrease the complexity of the pore boundary.[26] Probability entropy can describe the directionality of pores in 2D space. The value of probability entropy ranges from 0 to 1, and a higher value of probability entropy indicates a more random direction for pores.

4. RESULTS

4.1. Geochemistry and Mineral Composition. The TOC contents of our samples are relatively high (Table 1), ranging from 0.97% to 4.58% with an average of 3.03%. The high OM maturity in our samples (ER$_o$ > 2.0%), indicates that these shales are highly overmature. These overmature samples
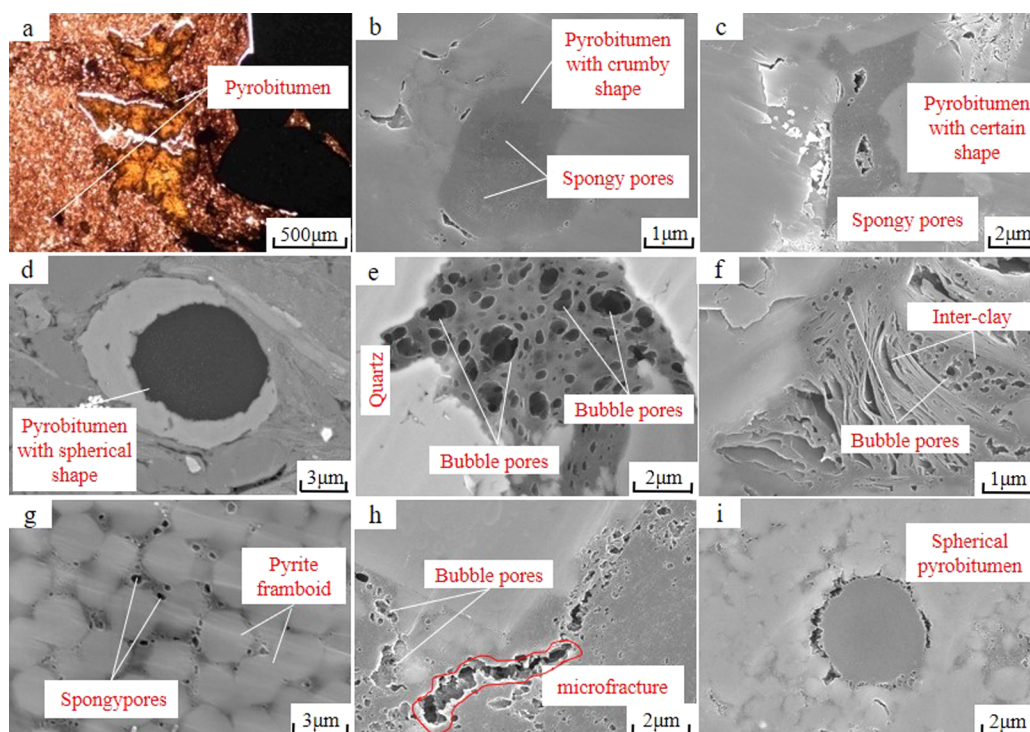
Figure 2. Characteristics of OM of the Wufeng−Longmaxi shale under an optical microscope and SEM. (a) Brownish black pyrobitumen, sample D1-1. (b) Spongy pores are developed in crumby-shaped pyrobitumen, sample H1-1. (c) Spongy pores are developed in pyrobitumen with a certain shape, sample H1-1. (d) Spherical-shaped pyrobitumen is filled in a fossil cavity, sample J2-1. (e) Bubble pores are developed in pyrobitumen, sample J1-1. (f) Bubble pores are developed in pyrobitumen filled in interclay, sample C1-2. (g) Spongy pores are developed in pyrite framboids, sample H1-1. (h) Superlarge bubble pores form a microfracture, sample C1-2. (i) microfractures are developed between spherical pyrobitumen and the surrounding minerals.

mainly consist of quartz (31−75%) and clay minerals (2− 52%), followed by carbonate minerals (0−63%), and pyrite (1−6%). For clay minerals, illite is dominant, followed by chlorite and a small amount of an illilite/smectite mixed layer (Table 1).

4.2. Identification of OM Types.
The kerogens in Wufeng−Longmaxi shales have endured strong physiochemical changes, which makes it difficult to differentiate kerogen components or solid bitumen. However, some researchers have made useful attempts. For example, Loucks and Reed[47] proposed several petrographic criteria to identify kerogen and solid bitumen, and abundant spongy pores are commonly observed in solid bitumen. Zhang et al.[27] identified algal, bacteria-like aggregates and spherical kerogen from the Wufeng−Longmaxi shale. From a comprehensive review of the published literature, two kinds of pyrobitumen and four kinds of kerogen were determined in this study.

4.2.1. Pyrobitumen and Related Pores.
Pyrobitumen is the most common OM type in the Wufeng−Longmaxi shale. Solid bitumen is believed to be a residual product of kerogen after hydrocarbon generation, which contains a partially insoluble fraction, whereas pyrobitumen generally refers to the largely insoluble residue after the transformation of retained oil to gas.[48] There have been some debates about the boundary of bitumen and pyrobitumen;[34] we tend to believe the view that most of the higher-molecular-weight retained oil has been transferred to gas at a maturity of ER_o exceeding 1.5%, and bitumen is insoluble at this stage.[34] Therefore, solid bitumen is classified as pyrobitumen in our samples.

Under an optical microscope, pyrobitumen is generally brownish black (Figure 2a). Compared with an optical microscope, FE-SEM has a higher resolution; thus, pyrobitumen can be more easily identified in SEM images. Generally, solid bitumen has no specific shape and fills in the interpartical (Inter P) pores between minerals and/or fossil cavities under SEM.[6,47] SEM observations found two kinds of pyrobitumen types in the Wufeng−Longmaxi shale. (1) Pyrobitumen with certain shape: this type of pyrobitumen is crumby and spherical-shaped (Figure 2b−d), which fills in dissolution pores and fossil cavities. (2) Pyrobitumen with no fixed shape: it mainly fills in the Inter P pores between granular minerals (Figure 2e), interclay pores (Figure 2f), and intercrystal pores (Figure 2g).

Pores are very common in pyrobitumen without a fixed shape. Based on the pore characteristics, bubbles and spongy pores are observed (Figure 2b,c). Bubble pores are nearly circular or elliptical, which generally have large pore sizes ranging from 100 to 800 nm (Figure 2b,c). The size of some superlarge bubble pores can reach to 1000 nm and even form microfractures occasionally (Figure 2e,h). These superlarge pores are usually suggested to be formed by the merging of multiple subpores.[49] These subpores are interconnected in 3D space resulting from the bitumen cracking to oil and gas,[47] which can effectively enhance the pore connectivity. Spongy pores are generally smaller (10−200 nm) compared to bubble pores and have rounded and subrounded shapes (Figure 2b,e). It is suggested that spongy pores are formed as a result of gas generation at high stages of maturation.[47]

Two types of pyrobitumen with a certain shape can be observed in our samples: crumby-shaped (Figure 2b,c) and spherical-shaped (Figure 2d,i). Crumby-shaped pyrobitumen has a clear edge in contact with the surrounding minerals, and
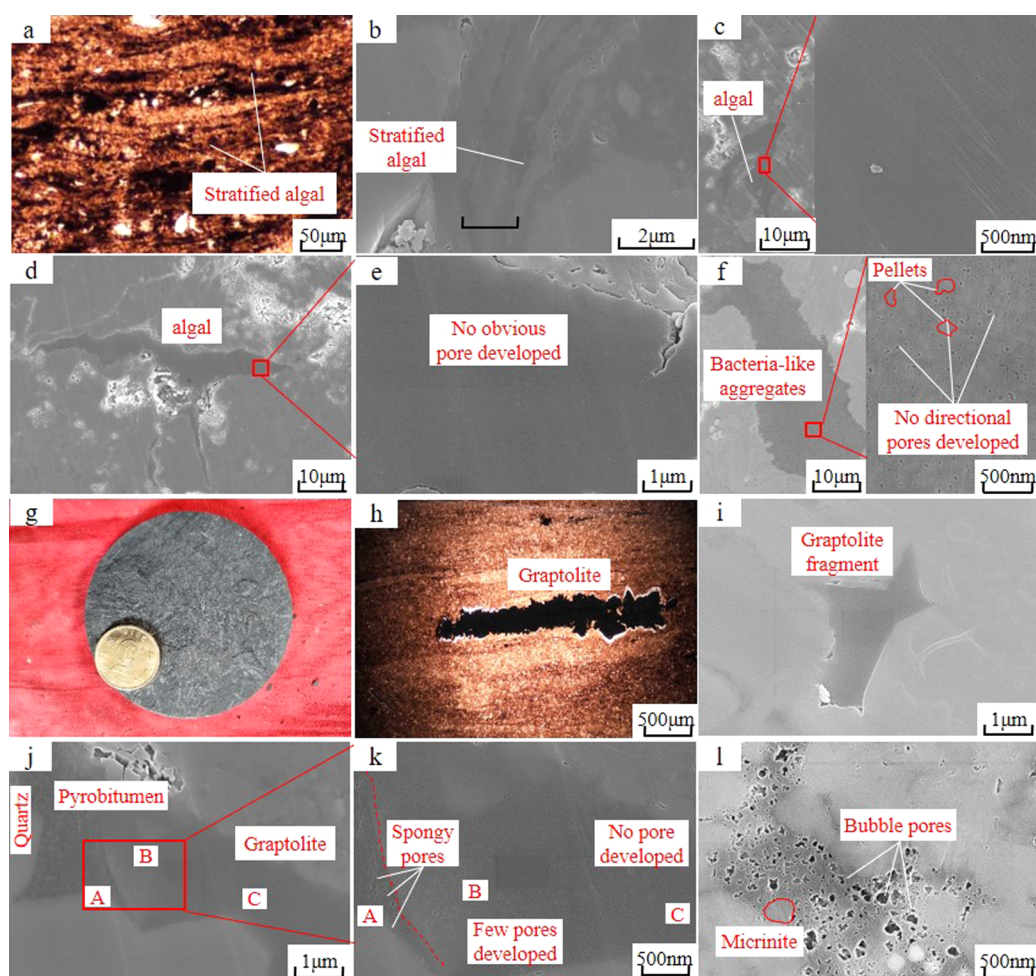
Figure 3. SEM images of kerogen of the Wufeng−Longmaxi shales. (a) Filament-shaped algal, sample Z1-1. (b) Floccule-shaped algal, sample W1-1. (c) Type II of algal has a unique shape with a length longer than 10 μm, sample Z1-2. (d, e) No obvious pores are developed in algal with unique shale, sample Z1-2. (f) Abundant quasi-spherical bacteria (pellets) are developed in bacteria-like aggregates and mesopores are observed, sample N1-3. (g) Large numbers of graptolites are observed in a hand specimen sample, sample W1-1. (h) Graptolite is black under an optical microscope with sharp outlines and a smooth surface, sample D1-1. (i) A graptolite fragment is observed in an SEM image, sample N1-3. (j, k) nearly no or very few OM pores are observed in graptolite fragments, sample W1-2. (l) Micrinite coexists with pyrobitumen characterized by a subrounded shape, sample C1-3.

the OM particles have a relatively small particle size (<10 μm). A large number of spongy pores are observed in crumby-shaped pyrobitumen with sizes ranging from 10 to 80 nm, whereas there are few bubble pores in them. Spherical pyrobitumen is only preserved in a few samples. Compared with the other pyrobitumen, spherical pyrobitumen is characterized as follows. (a) The shape of spherical pyrobitumen is spherical or hemispherical under SEM (Figure 2d,i) with diameters ranging from 4 to 8 μm. Previous studies suggested that the spherical OM may be algae cystocarp, acritarchs, and single-cell planktonic algae,[29,50] but we tend to believe that this spherical OM is pyrobitumen due to its circular shape. (b) The spherical bitumen has a typical two-layer structure although some of it is not obvious. OM in the core is homogeneous, whereas the outlines of this OM have a clear boundary in contact with the surrounding minerals (Figure 2d,e). In addition, some obvious differences are observed between the core and periphery of spherical pyrobitumen. Specifically, bubble pores are developed in the periphery, whereas no obvious pore is observed in the core of this OM (Figure 2i). Pores in the periphery of the spherical pyrobitumen are nonuniform, characterized by a bubble shape.

After careful observation, we tend to believe that the core and periphery of this OM are pyrobitumen. The reasons are that (1) the outline of peripheral pyrobitumen retains a trace of hydrocarbon migration (Figure 2d,i) and (2) the circular shape of this OM particle may indicate that the circular space originates from a fossil cavity before oil filling.

4.2.2. Types of Kerogen and Related Pores. 4.2.2.1. Algal Fragments. At least two types of algal fragments are identified in our samples. The first type is characterized by filament or floccules shapes as seen under an optical microscope and SEM (Figure 3a,b), and no obvious pore is observed within them. The biological origin of these algal fragments are still unclear. The other type of algal fragment is different from the first type in two aspects. First, it has a unique shape with a length generally greater than 10 μm (most samples have lengths up to 20 μm) (Figure 3c−e). Second, very few pores are observed in these samples. Since a clear boundary between surrounding minerals and this OM particle and secondary enlargement of surrounding quartz are not observed, we tend to believe that this type of algal fragment is kerogen rather than pyrobitumen. In addition, the size of these kerogens are usually more than 20 μm; if they are the Inter P pores filled by bitumen, the pores

Table 2. Relative Content of Different OM Types^a

Well	pyrobitumen (%)		algal fragments (%)	bacteria-like aggregates (%)	graptolites (%)	micrinites (%)
	without fixed shape	with certain shape				
CS#1	(82−95)/88.5	(0−5)/2.5	(0−5)/2.5	0	0	(5−8)/6.5
Z#1	(55−85)/67.5	(0−5)/2	(10−40)/23.75	(0−15)/5.75	0	(2−5)/4.25
NX#1	(45−80)/63.33	(0−8)/1.5	(15−30)/23.3	(0−20)/6.67	(2−10)/5.67	(0−3)/1
H#1	(60−75)/67.5	(0−5)/1.67	(5−35)/20	(0−5)/2.5	(5−8)/6.5	(0−10)/5
W#1	(53−75)/64	(0−5)/2.5	(10−40)/25	(0−2)/1	(0−5)/2	5

^{a}The relative content of graptolites may be underestimated; the slant represents not detected.

are hardly preserved during compaction in the diagenetic stage. The clear outlines of algal fragments, very few pores within them, and the size of generally more than 20 μm are typical features that differ from other OM types.

4.2.2.2. Bacteria-Like Aggregates. They comprise the aggregates of abundant quasi-spherical bacteria (pellets) (Figure 3f). Pellets can be identified in SEM images (Figure 3f) with a size generally ranging from 100 to 200 nm. Because of strong compaction, pellets are merged together and it is difficult to distinguish bacteria-like aggregates from pyrobitumen and algal fragments, especially in low-resolution SEM images. However, we suggest that the bacteria-like aggregates can be distinguished from other OM types in two aspects. First, the surfaces of the bacteria-like aggregates under an SEM are not smooth and many burrs exist (Figure 3f). Second, they consist of many rounded or subrounded pellets as seen in high-resolution SEM images (Figure 3f). A large number of pores are observed between pellets, which are characterized by irregular and angular shapes with sizes ranging from 5 to 30 nm. Most pores in bacteria-like aggregates have no direction, which is obviously different from the bubble and spongy pores in pyrobitumen.

4.2.2.3. Graptolites. Graptolites are the most common OM type in our hand specimen samples (Figure 3g), which are considered as the markers for the Wufeng−Longmaxi shale.[37] They mainly exist in the form of flattened carbonaceous films that are parallel to the beddings,[51] which are black under optical an microscope with sharp outlines and a smooth surface (Figure 3h). It is difficult to observe an entire graptolite under an SEM because they mainly exist in fragments with a size usually ranging from 1 to 3 μm under an SEM (Figure 3i). We also observed a close relationship between graptolite and pyrite/pyrobitumen (Figure 3j), which was also found in previous research.[27] Nearly no or very few OM pores were observed in graptolites (Figure 3i,k), which could be attributed to the chemical properties of graptolites that mainly consist of aromatic compounds with aliphatic groups, making graptolites similar to type III kerogen.[52] However, there is still a possibility that micropores can be developed in graptolites. This is because graptolite tends to generate gas due to its chemistry being similar to that of type III kerogen, and some pores that are invisible under SEM may exist in H-poor humic coals.[52]

4.2.2.4. Micrinite. It is very difficult to distinguish micrinite from microcrystalline quartz under an optical microscope.[32] Micrinite is considered as the residue of bitumen after the oil-prone kerogen macerals have been converted to hydrocarbons; thus, micrinite is a common OM type when shales are highly overmature. In our samples, micrinite usually coexists with pyrobitumen (Figure 3l), which is characterized by a subrounded shape with a size generally ranging from 100 to

400 nm. It is noted that no pores are observed in micrinite (Figure 3l).

5. DISCUSSION

5.1. Pore Development in Typical OM. According to SEM observation, the development of pores within OM is different. To better reflect the pore development in different types of OM, a PCAS analysis was applied to quantitatively characterize the property of pores for typical OM particles (Table 2). It has been calculated that more than 90% of pyrobitumen is pyrobitumen without a fixed shape by using an area estimation method. Taking a pyrobutumen without a fixed shape as an example (Figure 4a), it has a high surface porosity
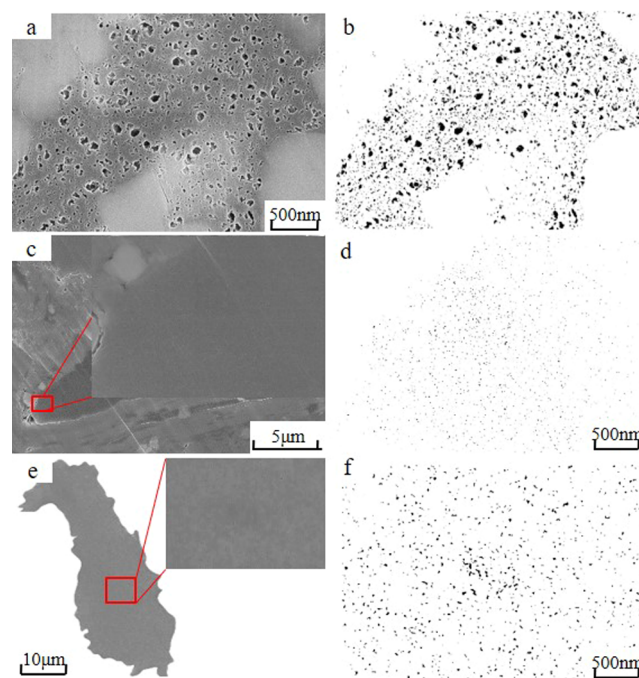

Figure 4. Typical OM types (left) and corresponding processing images (right) by PCAS analysis.

of up to 8.21%. The high values of the form factor (0.65) and probability entropy (0.978) indicate that the shape of this pyrobitumen is regular without directionality, providing a good condition for shale gas preservation.Pyrobitumen without a fixed shape hosts pores with sizes ranging from 6 to 78 nm (averaging 17 nm), which mostly range from 2 to 30 nm (Figure 5). Within the above range, the frequency of pores decreased with an increase in pore diameter (Figure 5). An algal fragment is the secondmost abundant OM type. Nearly no or few pores are observed in algal fragments (Figure 4b). Figure 4b shows a typical algal fragment observed in our
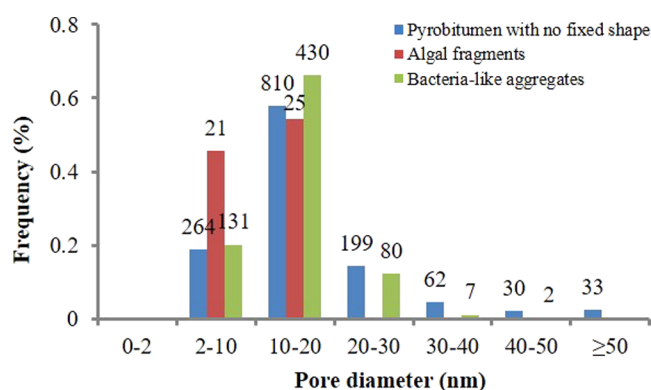
Figure 5. Pore size distribution of typical OM type hosted pores.

sample, and a PCAS analysis demonstrates that the surface porosity of an algal fragment can be as low as 0.72%. The high values of the form factor (0.68) and probability entropy (0.928) imply that pores in the algal fragment are regular without directionality, which could possibly be due to the small pore size of pores in the algal fragment. A PCAS analysis shows that the pores in an algal fragment are small, ranging from 7 to 16 nm with an average size of 10 nm (Figure 5). Bacteria-like aggregates are not common in the Wufeng−Longmaxi shales, which only comprise less than 5% of OM. A PCAS analysis demonstrates that the surface porosity of bacteria-like aggregates can reach 2.0% (Figure 4c). The pore size of bacteria-like aggregate hosted pores is usually small, mainly distributed in the range of 7−45 nm with an average of 14 nm. The high values of the form factor (0.68) and probability entropy (0.967) indicate that the pores in bacteria-like aggregate hosted pores are regular without directionality. Within the mesopore range, the frequency of these pores increase first and then decrease with an increase in pore diameter (Figure 5). It is noted that pores developed in pyrobitumen without a fixed shape are obviously different in the samples, which can be attributed to the influence of different mineral compositions (see discussion in section 5.2).

In the previous section, FE-SEM observations and a PCAS analysis were used to investigate the visible pores in OM. However, the development pores with a size less than 5 nm (invisible pores) in shales cannot be detected. Therefore, CO_2 and N_2 adsorption experiments were conducted to study the pore characteristics of shales with different OM types. The relative content of different OM types was calculated by using

an area estimation method (Table 2), which shows that pyrobitumen without a fixed shape is the dominant OM type and algal fragment is the second most abundant in the Wufeng−Longmaxi shale. The results of CO_2 and N_2 adsorption are given in Table 3.

Our results show that OM is beneficial for the development of micropores and meso-/macropores in shales (Figure 6a,d). Specifically, a weak to moderate positive correlation of TOC, pyrobitumen without a fixed shape, and SSA and PV of micropores is observed (Figure 6a,b), indicating that pyrobitumen without a fixed shape may contain many micropores. Moreover, TOC and pyrobitumen without a fixed shape are weakly to moderately positively correlated with meso-/macropores (Figure 6c,d), which supports our observation that large numbers of mesopores are developed in pyrobitumen without a fixed shape. It is noted that there is a moderate negative correlation between carbonates and the SSA as well as PV of pores including micropores and meso-macropores (Figure 6e-g), which means that carbonates are unfavorable for pore development. This is because carbonates such as calcite and dolomite are cements in the Wufeng−Longmaxi shales, which can block the pore space, resulting in a decrease of porosity. The significant positive correlation of quartz and TOC (Figure 6i) suggests that most quartz has an organic origin, which is consistent with previous research.[18] In addition, clay is moderately positively correlated with SSA of meso-/macropores (Figure 6g), confirming that meso-/macropores are also developed in clays.

5.2. Effect of Mineralogy on OM Pores. In the previous section, we found that pyrobitumen without a fixed shape hosted pores is the most common pore type. Therefore, an investigation of OM pores should focus on the pyrobitumen without a fixed shape rather than other OM types, and the presence or absence of pores in pyrobitumen without a fixed shape can be evaluated based on the pore heterogeneity resulting from the variations of mineral composition. In a previous study, Curtis et al.[4] observed that the distance between porous OM and nonporous OM is a few micrometers. The reason for this is that the porous OM is protected by rigid minerals such as quartz. A similar result has also been reported by other researchers.[6,53,54] For example, Zhang et al.[27] suggested that silica-rich shale contains abundant OM-hosted pores compared to clay-rich shale.

A holistic understanding shows that pyrobitumen without a fixed shape hosted pores are prone to be preserved if they infill the interparticle space surroundings by quartz. At this point,

Table 3. Analysis Results of CO_2 and N_2 Adsorption

| well	sample	TOC (%)	pyrobitumen with no fixed shape (%)	algal fragments (%)	CO_2 adsorption		N_2 adsorption	
					SSA (m^2/g)	PV (cm^3/g)	SSA (m^2/g)	PV (cm^3/g)
CS#1	C1-2	4.20	3.44	0.21	15.79	0.0021	13.58	0.0358
	C1-3	4.36	4.14	0.00	15.76	0.0024	13.41	0.0356
Z#1	Z1-2	2.25	1.24	0.90	13.88	0.0021	17.20	0.0120
	Z1-3	2.36	2.01	0.24	12.85	0.0019	15.09	0.0100
	Z1-4	4.40	2.86	1.10	18.07	0.0031	19.73	0.0100
	Z1-5	3.71	2.41	0.74	18.34	0.0031	18.55	0.0080
NX#1	N1-1	3.16	2.05	0.95	10.13	0.0016	9.59	0.0060
	N1-2	4.40	3.52	0.66	13.64	0.0022	13.90	0.0100
	N1-3	1.82	0.82	0.46	8.35	0.0012	10.27	0.0070
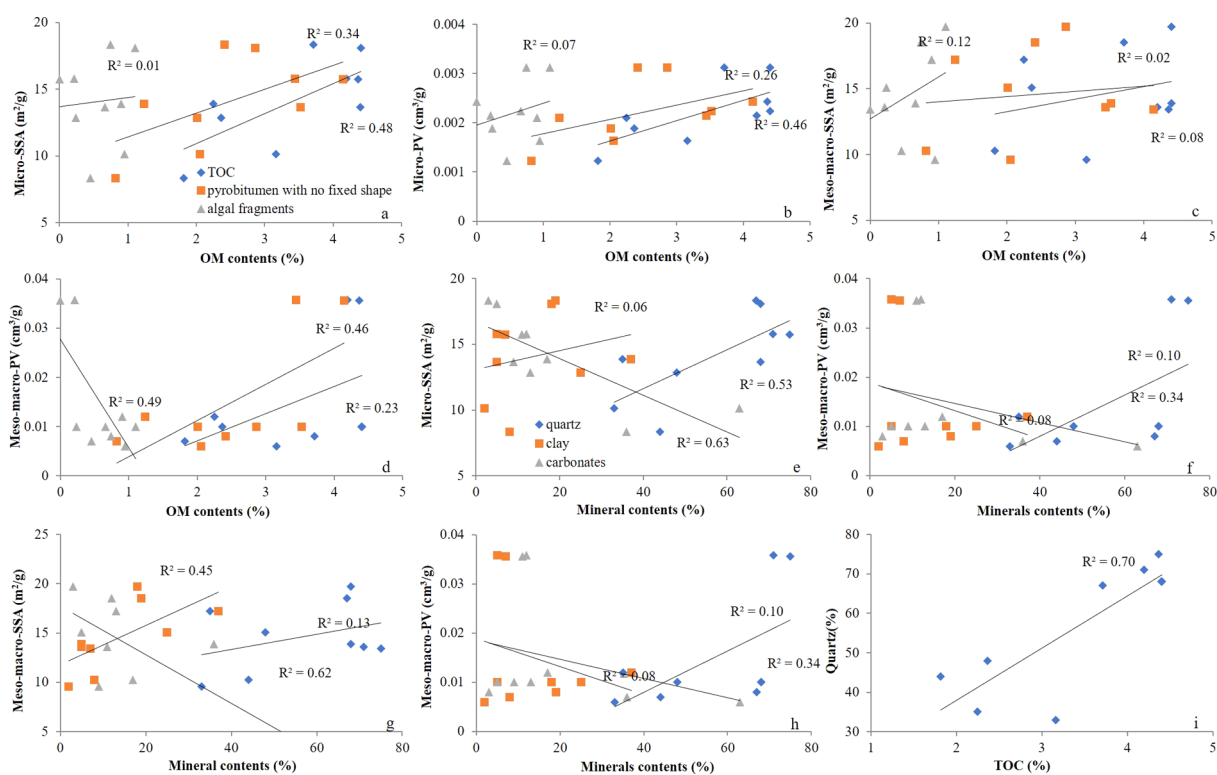
Figure 6. Correlation of OM types and SSA and PV of micro-/meso-/macropores of samples.

we present evidence based on the SEM images in order to focus on the underlying geological reasons and better assess the enrichment capacity for shale gas.

Four shale samples, including two quartz-rich samples (Z1-5 and H1-1) and two clay-rich samples (Z1-2 and H1-2), were selected to determine the impact of mineralogy on OM pore development (Table 1). The burial depth and OM maturity of the samples of the two groups (Z1-2, Z1-5 and H1-1, H1-2) are comparable, since the four samples are highly overmature. SEM images of the four samples are shown in Figure 7. Each sample includes (1) a low-magnification image that gives a general view of OM and its surrounding minerals, (2) an energy dispersive X-ray spectrum (EDS) to determine their mineralogy by the abundance of several major elements (e.g., C, O, Si, Al, Mg, Ca), and (3) a higher magnification (×100k and above) view of the OM to show possible pores in pyrobitumen without a fixed shape.

Figure 7a demonstrates a low-magnification view of a sample showing the relationship of OM and the surrounding minerals. Area scanning by EDS reveals that the surrounding minerals are mainly clays (Figure 7b). Figure 7c shows that only small amounts of pores are observed in this OM particle. As a comparison, more pores in pyrobitumen without a fixed shape are observed in quartz-rich shale (Figure 7d−f).

Figure 7g,l shows SEM images from a quartz-rich sample (53.5% quartz, H1-1) and a quartz-poorer sample (34%, quartz, H1-2); the two samples have similar clay mineral contents (Table 1). Note that abundant bubble pores are observed in the quartz-rich sample (Figure 6c) whereas very few pores are observed in the quartz-poorer sample (Figure 7l). These indicate that quartz is conductive to the preservation of pores in pyrobitumen without a fixed shape.

A PCAS analysis (Table 4) shows that pyrobitumen without a fixed shape in quartz-rich shale samples contains significantly

more pores compared to those in clay-rich shale samples. In other words, quartz-rich brittle shale will provide more visible SEM pores in pyrobitumen without a fixed shape compared to clay-rich ductile shale. Meantime, the lower value of form factor and probability entropy for clay-rich shale may imply that pores in pyrobitumen without a fixed shape in clay-rich shale are prone to be compacted and show more directions.

It should be noted that brittle minerals such as quartz, pyrite, and calcite can promote the preservation of pores in pyrobitumen without a fixed shape in different ways. Quartz can work as a rigid framework which effectively slows down the compaction and facilitates the preservation of pores.[53] When pyrobitumen fills into the interpartical spaces in quartz, pores in pyrobitumen can be well preserved. At the contact line of pyrobitumen and quartz, the pyrobitumen-hosted pores can be easily compacted and have an elongated shape (Figure 8a). Similarly to quartz, pyrite can also promote the preservation of pores. Pyrobitumen-hosted pores are widespread in pyrite framboids (Figure 8b). In addition, pyrobitmen within clay minerals also contains abundant bubble and spongy pores (Figure 8c). Carbonate minerals such as calcite and dolomite are considered to be brittle minerals, which are favorable for postfracturing;[55,56] however, the relationship between pyrobitumen-hosted pores and carbonates is unclear. Figure 8d shows a low-magnification view of a calcite-rich sample displaying the association between OM and surrounding minerals. Figure 8e shows that the OM particles are located at the right side of quartz and left side of calcite, and we observed that more pores are developed in pyrobitumen close to quartz compared with those close to calcite. Therefore, it seems reasonable to conclude that quartz is better for the preservation of pyrobitumen-hosted pores compared to carbonates.

Therefore, we conclude that the shale mineral composition has an effect on the preservation of pyrobitumen-hosted pores
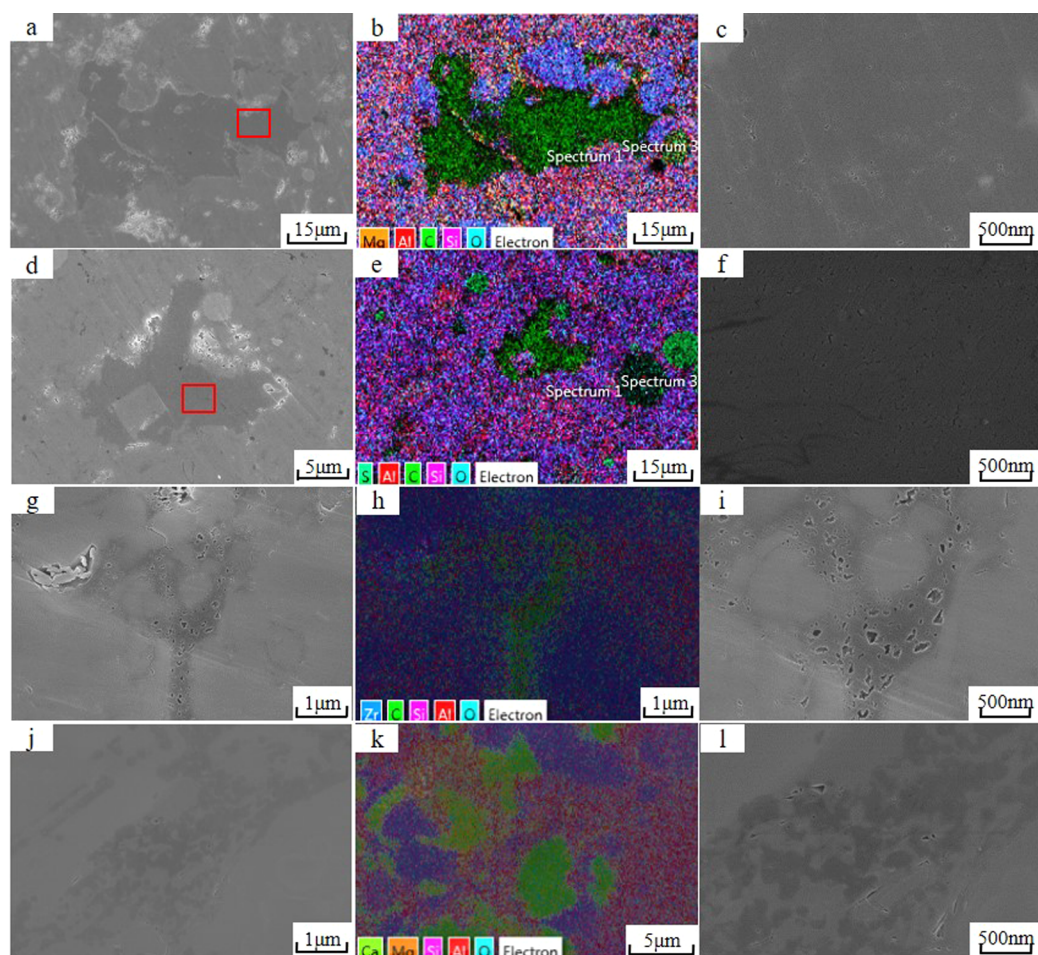
Figure 7. SEM images for clay-rich samples and quartz-rich samples with EDS area scans for the determination of the chemical composition of minerals. (a–c) Only a small amount of pores is observed in OM particles for clay-rich shale, sample Z1-2. (d–f) A large number of spongy pores are developed in pyrobitumen withouta fixed shape in quartz-rich shale, sample Z1-5. (g–i) Bubble pores are observed in quartz-rich shale, sample H1-1. (j–l) Very few pores are observed in a quartz-poorer sample, sample H1-2.

Table 4. PCAS Analysis Results of Four Samples

sample	plane porosity in OM (%)	pore number	form factor	probability entropy	pore development
Z1-2	0.14	23	0.56	0.797	few spongy pores
Z1-5	2.6	284	0.61	0.956	many spongy pores
H1-1	4.12	396	0.60	0.966	large number of bubble pores
H1-2					nearly no pores

and quartz-rich brittle shale contains more visible pores in pyrobitumen compared to clay-rich ductile shale.

5.4. Preservation of OM Pores in Wufeng–Longmaxi Shale. SEM observations show that the OM type is fundamental in deciding the OM pore development. Pores in kerogen are controlled by a combination of the property of OM, hydrocarbon expulsion efficiency ,and condensed degree, whereas pores in pyrobitumen are dominated by OM maturity.[57] OM maturity has an obvious impact on the formation, development, evolution, and preservation of OM pores. In general, OM pores begin to generate when OM maturity is in the mature stage (R_o ranging from 0.7% to 0.9%). With an increase in OM maturity, OM pores increase significantly and peak in the stage of R_o at 2.2%, and then OM

pores decrease gradually. When R_o reaches 3.5%, the carbonization of OM occurs, resulting in a sharp decrease or even disappearance of OM pores.[57−59] An R_o value of 4.0% is believed to be the maturity threshold of OM pore extinction.[57] The R_o value of Wufeng–Longmaxi shale in the Sichuan Basin usually ranges from 2.0% to 3.0%,[27,60] indicating that OM maturity is favorable for the formation and development of OM pores. In other words, OM maturity of Wufeng–Longmaxi shale is not the main factor influencing the difference in OM pore development in our samples.

The Wufeng–Longmaxi shale experienced mechanical compaction, pyrite cementation, and biologic opal recrystallization during early diagenesis, montmorillonite illitization, quartz overgrowth, and hydrocarbon generation during middle digenesis, and ankerite replacement and liquid hydrocarbon thermal cracking during late diagenesis.[60,62] An R_o value higher than 2.0% and illite crystallinity ranging from 0.27 to 0.37 indicates that the Wufeng–Longmaxi shale is in late diagenesis.[57,60] The diagenesis and changes in mineral composition induced by diagenesis will have an obvious impact on OM pore development.

The reduction of OM pores in the Wufeng–Longmaxi shale is due to the polycondensation of OM and compaction. The former is characterized by OM pores disappearing gradually with an R_o value higher than 3.5%, which is considered as the
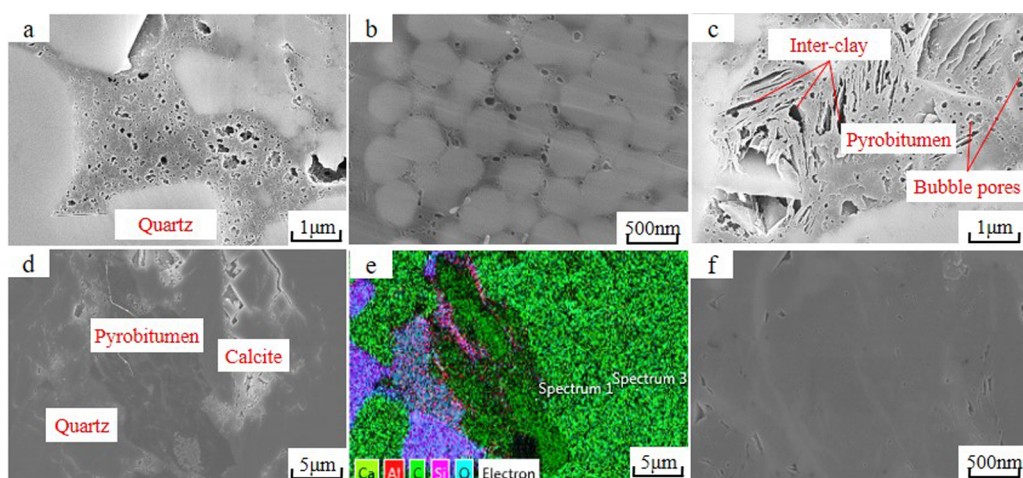
Figure 8. Relationship between pyrobitumen-hosted pores and the surrounding minerals. (a) Large numbers of bubble pores are observed in pyrobitumen surrounded by quartz, sample C1-3. (b) Pyrobitumen-hosted pores are well developed in pyrite framboids, sample J2-1. (c) Pyrobitmen within clay minerals contains abundant bubbles and spongy pores, sample C1-2. (d−f) More pores are observed in pyrobitumen close to quartz compared with those close to calcite, sample N1-1.
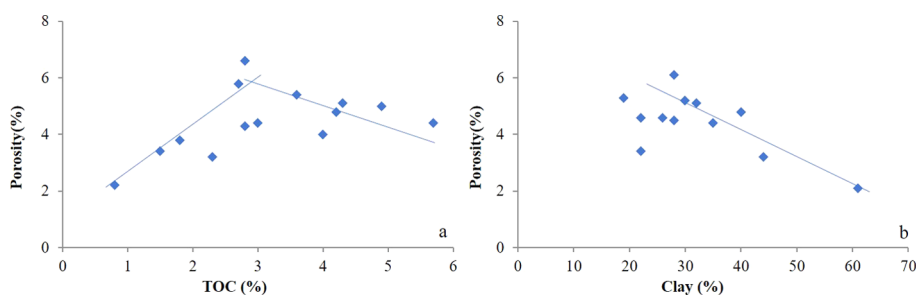

Figure 9. Relationship between TOC and porosity of shales from well JY2.

internal cause that results in the decrease of OM pores. The latter directly causes the densification of shale, which is believed to be the external cause. OM pores will be compacted and further reduced without a surrounding rigid mineral framework and pore fluid pressure, which directly results in a decrease in porosity and PV. In comparison, OM pores in clay-rich or OM-rich shale may be more easily compacted due to their high plasticity. Figure 9a shows that the TOC is positively associated with porosity with a TOC value of less than 3.0%, whereas an obvious negative relationship between them is obtained with a TOC value exceeding 3.0%. Figure 9b shows an obvious negative correlation of clay mineral contents and the porosity of shale. These findings indicate that a high content of clay minerals and TOC can strengthen the plasticity of shale, especially for clay-rich shale that lacks rigid minerals and fluid pressure; compaction has a strong impact on OM pores and then results in the reduction of porosity.

In addition, fluid pressure also has an obvious impact on the development of OM pores. Fluid pressure in pores will increase gradually with the generation of gas resulting from kerogen and resident oil thermal cracking. Under good sealing conditions, OM pores containing large amounts of gas are in overpressure or high pressure, which can effectively resist the compaction of overlying strata and regional structural stress and further promote the preservation of OM pores. In the overpressure system of the Fuling gas field and Dingshan region, OM pores in the Wufeng−Longmaxi shale show a large size and round or subround shape (Figure 2e), which is closely related to the increase in compressive strength of shales under overpressure. Especially for those OM pores surrounded by rigid minerals, OM pores in shale are very common, even when these shales are in deep and superdeep burial depth (Figures 2f, 3l, and 8a). Numerous studies have demonstrated that shales under overpressure or high-pressure conditions have a high porosity (>4.5%), a high surface porosity of OM (10%−40%), and a high gas content (>5.0 m^3/t).[63,64] Statistics show that shales under overpressure or high-pressure conditions have higher porosity compared with those under normal pressure (Figure 10). Therefore, abnormal fluid pressure (overpressure or high pressure) is favorable for the development of OM pores.

In conclusion, the formation and preservation of OM pores in the Wufeng−Longmaxi shale is mainly controlled by the OM type and diagenesis. The rigid mineral framework, including that formed by quartz recrystallization and pyrite cementation, and the pore-fluid pressure are favorable for the development of OM pores.

5.5. Significance of Pores in Pyrobitumen without Fixed Shape. Pyrobitumen makes the great contribution to gas storage for both free gas and adsorption gas because of its high porosity and high SSA.[65,66] For the Wufeng−Longmaxi shales, pores in pyrobitumen without a fixed shape contribute to most of the pores in OM. Pyrobitumen-hosted pores are associated with the transformation of retained oil to gas, and they are characterized by a round or subround shape at the initial formation stage. Then, these round or subround pores gradually change into an elliptical shape due to the increase of temperature and pressure at the late diagenesis stage.[67]
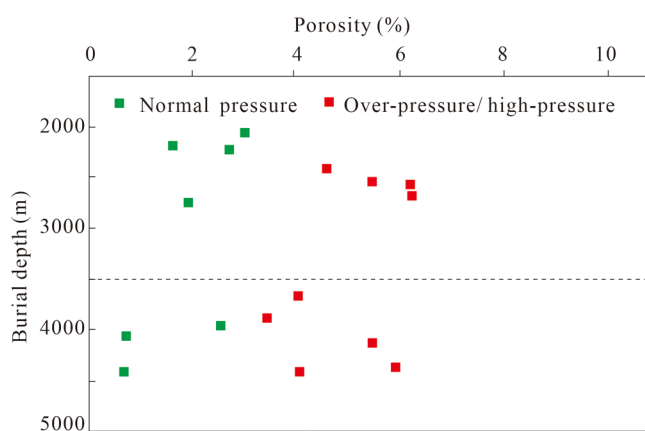
Figure 10. Comparison of porosity of shales at overpressure or high and normal pressures.

Therefore, the morphology of pyrobitumen-hosted pores is mainly controlled by the temperature and pressure of strata in theory. Generally, the pressure increases with the burial depth, and when the pressure is high enough, gas in shales will be released and pore pressure will be reduced and be restored to normal pressure.[68] For the overmature Wufeng−Longmaxi shale, the majority of released gas may be restored in pyrobitumen-hosted pores. The pyribitumen-hosted pores can store large amounts of gases, which builds up pore pressure and maintains the pore morphology of a round or subround shape. Therefore, the existence of abundant round- or subround-shaped pyrobitumen-hosted pores in shales may indicate the large amounts of gases that were preserved in pyrobitumen. Consequently, the properties of pyrobitumen-hosted pores, including pore size, pore morphology, and pore deformation degree, can reflect the pressure condition of the strata. Recent research demonstrated that shales with abundant bubble pores and round- or subround-shaped pyrobitumen hosted pores normally have a high gas content and shale gas production.[61] In our previous study, we observed a good positive correlation of the pore form factor and shale gas content when the burial depth of shale was more than 2500 m.[69] Thus, we suggested that the morphology of pyrobitumen-hosted pores can partially reflect the shale gas accumulation. A further investigation of pyrobitumen and related pores is essential for a better understanding of the shale gas accumulation.

6. CONCLUSION

In this study, shale samples from the Wufeng−Longmaxi Formation were collected in the Sichuan Basin to study the OM types and their related pore characteristics by using FE-SEM with EDS, a PCAS quantitative analysis, and gas adsorption experiments. We concluded the following.

(1) Pyrobitumen and kerogen have been identified by optical microscope and SEM observations. Pyrobitumen can be divided into pyrobitumen without a fixed shape and pyrobitumen with certain shape, whereas kerogen is classified as algal fragments, bacteria-like aggregates, graptolite, and micrinite. It is calculated that pyrobitumen is the major component of OM followed by algal fragments. SEM observations demonstrated that large amounts of pores are developed in pyrobitumen, whereas nearly no or few pores are observed in algal fragments.

(2) The mineral composition has an effect on the preservation of pores in pyrobitumen without a fixed shape. Quartz-rich brittle shale contains more pyrobitumen-hosted pores compared to clay-rich ductile shale. Moreover, quartz is better for the preservation of pyrobitumen-hosted pores compared to carbonates. The rigid mineral framework, including that formed by quartz recrystallization and pyrite cementation, and the pore-fluid pressure are favorable for the development of OM pores.

(3) Gas adsorption experiments demonstrated that pyrobitumen makes a great contribution to pore development, including micropores and meso-/macropores. Carbonates are unfavorable for pore development because they can block the pore as cements.

(4) The morphology of pyrobitumen-hosted pores can possibly reflect the shale gas accumulation. Further investigation of pyrobitumen and related pores is essential for a better understanding of the shale gas accumulation.

■ AUTHOR INFORMATION

Corresponding Author

Guoliang Xie − *School of Civil Engineering & Architechure, Tongling University, Tongling 244000, People's Republic of China; State Key Laboratory of Oil and Gas Reservoir Geology and Exploitation, Chengdu University of Technology, Chengdu 610059, People's Republic of China;* ⬤ orcid.org/0000-0002-2612-9238; Email: glxie1989@tlu.edu.cn

Author

Weiduo Hao − *Department of Earth & Atmospheric Sciences, University of Alberta, Edmonton, Alberta T6E 2E3, Canada;* ⬤ orcid.org/0000-0002-0486-424X

Complete contact information is available at:
https://pubs.acs.org/10.1021/acsomega.2c04497

Notes

The authors declare no competing financial interest.

■ ACKNOWLEDGMENTS

■ REFERENCES

(1) Zou, C. N.; Yang, Z.; Zhu, R. K.; Wu, S. K.; Fu, J. H.; Lei, D. W.; Hou, L. H.; Lin, S. H.; Pan, S. Q. Geologic significance and optimization technique of sweet spots in unconventional shale systems. *J. Asian Earth Sci.* **2019**, *178*, 3−19.

(2) Zou, C. N.; Yang, Z.; Sun, S. S.; Qun, Z.; Bai, W. J.; Liu, H. L.; Pan, S. Q.; Wu, S. T.; Yuan, Y. L. Exploring petroleum inside source kitchen": Shale oil and gas in Sichuan Basin. *Sci. China-Earth Sci.* **2020**, *50* (7), 903−920.

(3) Ma, X. H.; Wang, H. Y.; Zhou, S. W.; Feng, Z. Q.; Liu, H. L.; Guo, W. Insights into NMR response characteristics of shales and its

application in shale gas reservoir evaluation. *J. Nat. Gas Sci. Eng.* **2020**, *84*, 103674.

(4) Curtis, M. E.; Cardott, B. J.; Sondergeld, C. H.; Rai, C. S. Development of organic porosity in the Woodford Shale with increasing thermal maturity. *Int. J. Coal Geol.* **2012**, *103*, 26−31.

(5) Curtis, J. B.; Faure, G. Accumulation of organic matter in the Rome trough of the Appalachian basin and its subsequent thermal history. *AAPG BULL* **1997**, *81* (3), 424−437.

(6) İnan, S.; Al Badairy, H.; İnan, T.; Al Zahrani, A. Formation and occurrence of organic matter-hosted porosity in shales. *Int. J. Coal Geol.* **2018**, *199*, 39−51.

(7) Li, Y. F.; Zhang, T. W.; Ellis, G. S.; Shao, D. Y. Depositional environment and organic matter accumulation of Upper Ordovician−Lower Silurian marine shale in the Upper Yangtze Platform, South China. *Palaeogeogr. Palaeocl.* **2017**, *466*, 252−264.

(8) Zhao, S. Z.; Li, Y.; Min, H. J.; Yu, Q.; Wang, Z. Q.; Deng, T.; Liu, H.; Chen, J. Mechanisms controlling organic matter enrichment in the Lower Silurian Longmaxi Formation black shale unit, southwestern margin of the Yangtze Platform, China. *Arab. J. Geosci.* **2019**, *12* (7), 252.

(9) Zhao, J. H.; Jin, Z. J.; Jin, Z. K.; Hu, Q. H.; Hu, Z. Q.; Du, W.; Yan, C. N.; Geng, Y. K. Mineral types and organic matters of the Ordovician-Silurian Wufeng and Longmaxi Shale in the Sichuan Basin, China: Implications for pore systems, diagenetic pathways, and reservoir quality in fine-grained sedimentary rocks. *Mar. Petrol. Geol.* **2017**, *86*, 655−674.

(10) Yang, F.; Xu, S.; Hao, F.; Hu, B. Y.; Zhang, B. Q.; Shu, Z. G.; Long, S. Y. Petrophysical characteristics of shales with different lithofacies in Jiaoshiba area, Sichuan Basin, China: Implications for shale gas accumulation mechanism. *Mar. Petrol. Geol.* **2019**, *109*, 394−407.

(11) Shu, Y.; Lu, Y. C.; Chen, L.; Wang, C.; Zhang, B. Q. Factors influencing shale gas accumulation in the lower Silurian Longmaxi formation between the north and South Jiaoshiba area, Southeast Sichuan Basin, China. *Mar. Petrol. Geol.* **2020**, *111*, 905−917.

(12) Tang, X. L.; Jiang, S.; Jiang, Z. X.; Li, Z.; He, Z. L.; Long, S. X.; Zhu, D. Y. Heterogeneity of Paleozoic Wufeng−Longmaxi formation shale and its effects on the shale gas accumulation in the Upper Yangtze Region, China. *Fuel* **2019**, *239*, 387−402.

(13) Zhang, K.; Song, Y.; Jiang, S.; Jiang, Z. X.; Jia, C. Z.; Huang, Y. Z.; Liu, X. X.; Wen, M.; Wang, X.; Li, X.; Wang, P. F.; Shan, C. G.; Liu, T. L.; Liu, W. W.; Xie, X. L. Shale gas accumulation mechanism in a syncline setting based on multiple geological factors: An example of southern Sichuan and the Xiuwu Basin in the Yangtze Region. *Fuel* **2019**, *241*, 468−476.

(14) Liu, K. Q.; Wang, L.; Ostadhassan, M.; Zou, J.; Bubach, B.; Rezaee, R. Nanopore structure comparison between shale oil and shale gas: examples from the Bakken and Longmaxi Formations. *Petrol. Sci.* **2019**, *16* (1), 77−93.

(15) Zhao, J. H.; Jin, Z. J.; Hu, Q. H.; Liu, K. Y.; Jin, Z. K.; Hu, Z. Q.; Nie, H. K.; Du, W.; Yan, C. N.; Wang, R. Y. Mineral composition and seal condition implicated in pore structure development of organic-rich Longmaxi shales, Sichuan Basin, China. *Mar. Petrol. Geol.* **2018**, *98*, 507−522.

(16) Jiao, K.; Yao, S. P.; Liu, C.; Gao, Y. Q.; Wu, H.; Li, M. C.; Tang, Z. Y. The characterization and quantitative analysis of nanopores in unconventional gas reservoir utilizing FESEM-FIB and image processing: An example from the lower Silurian Longmaxi Shale, upper Yangtze region, China. *Int. J. Coal Geol.* **2014**, *128−129*, 1−11.

(17) Jiao, K.; Yao, S. P.; Zhang, K.; Hu, W. X.; Cao, J. The evolution of nanopores and surface roughness in naturally matured coals in South China: An atomic force microscopy and image processing study. *Fuel* **2018**, *234*, 1123−1131.

(18) Ma, Y.; Zhong, N. N.; Cheng, L. J.; Pan, Z. J.; Dai, N.; Zhang, Y.; Liu, Y. Pore structure of the graptolite-derived OM in the Longmaxi Shale, southeastern Upper Yangtze Region, China. *Mar. Petrol. Geol.* **2016**, *72*, 1−11.

(19) Guan, Q. Z.; Lü, X. X.; Dong, D. Z.; Cai, X. Origin and significance of organic-matter pores in Upper Ordovician Wufeng-Lower Silurian Longmaxi mudstones, Sichuan Basin. *J. Petrol. Sci. Eng.* **2019**, *176*, 554−561.

(20) Xi, Z. D.; Tang, S. H.; Li, J.; Zhang, Z. Y.; Xiao, H. Q. Pore characterization and the controls of organic matter and quartz on pore structure: Case study of the Niutitang Formation of northern Guizhou Province, South China. *J. Nat. Gas Sci. Eng.* **2019**, *61*, 18−31.

(21) Chen, F. W.; Zheng, Q.; Ding, X.; Lu, S. F.; Zhao, H. Q. Pore size distributions contributed by OM, clay and other minerals in over-mature marine shale: A case study of the Longmaxi shale from Southeast Chongqing, China. *Mar. Petrol. Geol.* **2020**, *122*, 104679.

(22) Huang, C.; Ju, Y. W.; Zhu, H. J.; Lash, G. G.; Qi, Y.; Yu, K.; Feng, H. Y.; Ju, L. T.; Qiao, P. Investigation of formation and evolution of organic matter pores in marine shale by helium ion microscope: An example from the Lower Silurian Longmaxi Shale, South China. *Mar. Petrol. Geol.* **2020**, *120*, 104550.

(23) Wang, P. F.; Zhang, C.; Li, X.; Zhang, K.; Yuan, Y.; Zang, X. P.; Cui, W. J.; Liu, S. Y.; Jiang, Z. X. Organic matter pores structure and evolution in shales based on the he ion microscopy (HIM): A case study from the Triassic Yanchang, Lower Silurian Longmaxi and Lower Cambrian Niutitang shales in China. *J. Nat. Gas Sci. Eng.* **2020**, *84*, 103682.

(24) Wu, Y. Q.; Tahmasebi, P.; Lin, C. Y.; Dong, C. M. A comprehensive investigation of the effects of Organic-Matter pores on shale properties: A multicomponent and multiscale modeling. *J. Nat. Gas Sci. Eng.* **2020**, *81*, 103425.

(25) Teng, J.; Liu, B.; Mastalerz, M.; Schieber, J. Origin of organic matter and organic pores in the overmature Ordovician-Silurian Wufeng−Longmaxi Shale of the Sichuan Basin, China. *Int. J. Coal Geol.* **2022**, *253*, 103970.

(26) Yang, W.; Wang, Y. H.; Du, W.; Song, Y.; Jiang, Z. X.; Wang, Q. Y.; Xu, L.; Zhao, F. P.; Chen, Y.; Shi, F. L.; Yao, S. H.; Hou, H. D.; Xiong, S. L. Behavior of organic matter-hosted pores within shale gas reservoirs in response to differential tectonic deformation: Potential mechanisms and innovative conceptual models. *J. Nat. Gas Sci. Eng.* **2022**, *102*, 104571.

(27) Zhang, W. T.; Hu, W. X.; Borjigin, T.; Zhu, F. Pore characteristics of different organic matter in black shale: A case study of the Wufeng−Longmaxi Formation in the Southeast Sichuan Basin, China. *Mar. Petrol. Geol.* **2020**, *111*, 33−43.

(28) Zhang, Y. F.; Yu, B. S.; Pan, Z. J.; Hou, C. H.; Zuo, Q. W.; Sun, M. D. Effect of thermal maturity on shale pore structure: A combined study using extracted organic matter and bulk shale from Sichuan Basin, China. *J. Nat. Gas Sci. Eng.* **2020**, *74*, 103089.

(29) Nie, H. K.; Jin, Z. J.; Zhang, J. C. Characteristics of three organic matter pore types in the Wufeng−Longmaxi Shale of the Sichuan Basin, Southwest China. *Sci. Rep.* **2018**, *8* (1), 7014.

(30) Luo, Q. Y.; Hao, J. Y.; Skovsted, C. B.; Xu, Y. H.; Liu, Y.; Wu, J.; Zhang, S. N.; Wang, W. L. Optical characteristics of graptolite-bearing sediments and its implication for thermal maturity assessment. *Int. J. Coal Geol.* **2018**, *195*, 386−401.

(31) Tian, H.; Pan, L.; Xiao, X. M.; Wilkins, R. W. T.; Meng, Z.; Huang, B. J. A preliminary study on the pore characterization of Lower Silurian black shales in the Chuandong Thrust Fold Belt, southwestern China using low pressure N_2 adsorption and FE-SEM methods. *Mar. Petrol. Geol.* **2013**, *48*, 8−19.

(32) Chen, Z. Y.; Song, Y.; Jiang, Z. X.; Liu, S. B.; Li, Z.; Shi, D. S.; Yang, W.; Yang, Y. D.; Song, J. N.; Gao, F. L.; Zhang, K.; Guo, X. B. Identification of organic matter components and organic pore characteristics of marine shale: A case study of Wufeng−Longmaxi shale in southern Sichuan Basin, China. *Mar. Petrol. Geol.* **2019**, *109*, 56−69.

(33) Yang, C.; Xiong, Y. Q.; Zhang, J. C. A comprehensive re-understanding of the OM-hosted nanopores in the marine Wufeng−Longmaxi shale formation in South China by organic petrology, gas adsorption, and X-ray diffraction studies. *Int. J. Coal Geol.* **2020**, *218*, 103362.

(34) Mastalerz, M.; Drobniak, A.; Stankiewicz, A. B. Origin, properties, and implications of solid bitumen in source-rock reservoirs: A review. *Int. J. Coal Geol.* **2018**, *195*, 14−36.

(35) Guo, X. W.; Qin, Z. J.; Yang, R.; Dong, T.; He, S.; Hao, F.; Yi, J. Z.; Shu, Z. G.; Bao, H. Y.; Liu, K. Y. Comparison of pore systems of clay-rich and silica-rich gas shales in the lower Silurian Longmaxi formation from the Jiaoshiba area in the eastern Sichuan Basin, China. *Mar. Petrol. Geol.* **2019**, *101*, 265−280.

(36) Wang, K.; Orth, C. J.; Attrep, J. R. M.; Chatterton, B. D. E.; Wang, X. F.; Li, J. J. The great latest Ordovician extinction on the South China Plate: Chemostratigraphic studies of the Ordovician-Silurian boundary interval on the Yangtze platform. *Palaeogeogr. Palaeocl.* **1993**, *104* (1), 61−79.

(37) Chen, X.; Rong, J. Y.; Li, Y.; Boucot, A. J. Facies patterns and geography of the Yangtze region, South China, through the Ordovician and Silurian transition. *Palaeogeogr. Palaeocl.* **2004**, *204* (3), 353−372.

(38) Ye, Y. H.; Liu, S. G.; Ran, B.; Luba, J.; Wang, S. Y.; Sun, W.; Yang, D.; Luo, C. Characteristics of black shale in the Upper Ordovician Wufeng and lower Silurian Longmaxi formations in the Sichuan Basin and its periphery, China. *Aust. J. Earth Sci.* **2017**, *64* (5), 667−687.

(39) Guo, X. S.; Li, Y. P.; Borjigen, T.; Wang, Q.; Yuan, T.; Shen, B. J.; Ma, Z. L.; Wei, F. B. Hydrocarbon generation and storage mechanisms of deep-water shelf shales of Ordovician Wufeng Formation−Silurian Longmaxi Formation in Sichuan Basin, China. *Petrol. Explor. Dev.* **2020**, *47* (1), 204−213.

(40) Gao, J.; Zhang, J. K.; He, S.; Zhao, J. X.; He, Z. L.; Wo, Y. J.; Feng, Y. X.; Li, W. Overpressure generation and evolution in Lower Paleozoic gas shales of the Jiaoshiba region, China: Implications for shale gas accumulation. *Mar. Petrol. Geol.* **2019**, *102*, 844−859.

(41) Jacob, H. Classification, structure, genesis and practical importance of natural solid oil bitumen ("migrabitumen"). *Int. J. Coal Geol.* **1989**, *11* (1), 65−79.

(42) Wang, Y.; Liu, L. F.; Chong, H. F. Gas Adsorption Characterization of Pore Structure of Organic-rich Shale: Insights into Contribution of Organic Matter to Shale Pore Network. *Nat. Resour. Res.* **2021**, *30* (3), 2377−2395.

(43) Mastalerz, M.; Schimmelmann, A.; Drobniak, A.; Chen, Y. Y. Porosity of Devonian and Mississippian New Albany Shale across a maturation gradient: Insightsfromorganicpetrology, gas adsorption, and mercury intrusion. *AAPG BULL* **2013**, *97* (10), 1621−1643.

(44) Wang, Y.; Chen, H. F.; Hu, Q. H.; Liu, L. F.; Jia, L. B.; Gao, S. S. Pore structure heterogeneity of Wufeng−Longmaxi shale, Sichuan Basin, China: Evidence from gas physisorption and multifractal geometries. *J. Petrol. Sci. Eng.* **2021**, *208*, 109313.

(45) Liu, C.; Shi, B.; Zhou, J.; Tang, C. S. Quantification and characterization of microporosity by image processing, geometric measurement and statistical methods: Application on SEM images of clay materials. *Appl. Clay Sci.* **2011**, *54* (1), 97−106.

(46) Jiao, K.; Yao, S. P.; Zhang, K.; Hu, W. X.; Cao, J. The evolution of nanopores and surface roughness in naturally matured coals in South China: An atomic force microscopy and image processing study. *Fuel* **2018**, *234*, 1123−1131.

(47) Loucks, R. G.; Reed, R. M.; Ruppel, S. C.; Jarvie, D. M. Morphology, Genesis, and Distribution of Nanometer-Scale Pores in Siliceous Mudstones of the Mississippian Barnett Shale. *J. Sediment. Res.* **2009**, *79* (12), 848−861.

(48) Hackley, P. C.; Cardott, B. J. Application of organic petrography in North American shale petroleum systems: A review. *Int. J. Coal Geol.* **2016**, *163*, 8−51.

(49) Mathia, E. J.; Bowen, L.; Thomas, K. M.; Aplin, A. C. Evolution of porosity and pore types in organic-rich, calcareous, Lower Toarcian Posidonia Shale. *Mar. Petrol. Geol.* **2016**, *75*, 117−139.

(50) Pang, Q.; Hu, G.; Jiao, K.; Tan, X. C.; Liu, H.; Ye, Y. H.; Yan, S.; Zhao, D. F. Characteristics of organic pores and composition of bio-precursors in the Wufeng and Longmaxi Formation shales, Southern Sichuan Basin, China. *Energy Explor. Exploit.* **2018**, *36* (4), 645−664.

(51) Borjigin, T.; Shen, B. J.; Yu, L. J.; Yang, Y. F.; Zhang, W. T.; Tao, C. C.; Xi, B. B.; Zhang, Q. Z.; Bao, F.; Qin, J. Z. Mechanisms of shale gas generation and accumulation in the Ordovician Wufeng−Longmaxi Formation, Sichuan Basin, SW China. *Petrol. Explor. Dev.* **2017**, *44* (1), 69−78.

(52) Tulay, Y.; Inan, A. A. H.; Koseoglu, O. R. Chemometrics-Based Analytical Method Using FTIR Spectroscopic Data to Predict Diesel and Diesel/Diesel Blend Properties. *Energy Fuel* **2016**, *30*, 5525−5536.

(53) Fishman, N. S.; Hackley, P. C.; Lowers, H. A.; Hill, R. J.; Egenhoff, S. O.; Eberl, D. D.; Blum, A. E. The nature of porosity in organic-rich mudstones of the Upper Jurassic Kimmeridge Clay Formation, North Sea, offshore United Kingdom. *Int. J. Coal Geol.* **2012**, *103*, 32−50.

(54) Bernard, S.; Wirth, R.; Schreiber, A.; Schulz, H. M.; Horsfield, B. Formation of nanoporous pyrobitumen residues during maturation of the Barnett Shale (Fort Worth Basin). *Int. J. Coal Geol.* **2012**, *103*, 3−11.

(55) Jarvie, D. M.; Hill, R. J.; Ruble, T. E.; Pollastro, R. M. Unconventional shale-gas systems: The Mississippian Barnett Shale of north-central Texas as one model for thermogenic shale-gas assessment. *AAPG Bull.* **2007**, *91* (4), 475−499.

(56) Kang, Y.; Shang, C.; Zhou, H.; Huang, Y.; Zhao, Q.; Deng, Z.; Wang, H.; Ma, Y. Z. Mineralogical brittleness index as a function of weighting brittle minerals-from laboratory tests to case study. *J. Nat. Gas Sci. Eng.* **2020**, *77*, 103278.

(57) Borjigin, T.; Lu, L. F.; Yu, L. J.; Zhang, W. T.; Pan, A. Y.; Shen, B. J.; Wang, Y.; Yang, Y. F.; Gao, Z. W. Formation, preservation and connectivity control of organic pores in shale. *Petrol. Explor. Dev.* **2021**, *48* (4), 687−699.

(58) Bernard, S.; Horsfield, B.; Schulz, H. M.; Wirth, R.; Schreiber, A.; Sherwood, N. Geochemical evolution of organic-rich shales with increasing maturity: a STXM and TEM study of the Posidonia Shale (lower Toarcian, northern Germany). *Mar. Petrol.Geol.* **2012**, *31*, 70−89.

(59) Wei, M. M.; Zhang, L.; Xiong, Y. Q.; Peng, P. A. Main factors influencing the development of nanopores in over-mature, organic-rich shales. *Int. J. Coal Geol.* **2019**, *212*, 103233.

(60) Liu, S. G.; Ma, W. X.; Jansa, L.; Huang, W. M.; Zeng, X. L.; Zhang, C. J. Characteristics of the shale gas reservoir rocks in the Lower Silurian Longmaxi Formation, East Sichuan Basin, China. *Energy Explor. Exploit.* **2013**, *31*, 187−219.

(61) Gao, P.; Xiao, X. M.; Hu, D. F.; Lash, G. G.; Liu, R. B.; Cai, Y. D.; Wang, Z. H.; Zhang, B. Y.; Yuan, T.; Liu, S. Y. Effect of silica diagenesis on porosity evolution of deep gas shale reservoir of the Lower Paleozoic Wufeng−Longmaxi formations, Sichuan Basin. *Mar. Petrol. Geol.* **2022**, *145*, 105873.

(62) Qiu, Z.; Liu, B.; Lu, B.; Shi, Z. S.; Li, Z. Y. Mineralogical and petrographic characteristics of the Ordovician-Silurian Wufeng−Longmaxi Shale in the Sichuan Basin and implications for depositional conditions and diagenesis of black shales. *Mar. Petrol.Geol.* **2022**, *135*, 105428.

(63) Nie, H. K.; LI, P.; Dang, W.; Ding, J. H.; Sun, C. X.; Liu, M.; Wang, J.; Du, W.; Zhang, P. X.; Li, D. H.; Su, H. K. Enrichment characteristics and research directions of deep shale gas: A case study of the Ordovician Wufeng-Silurian Longmaxi shale in the Sichuan Basin and its surrounding areas, China. *Petrol. Explor. Dev.* **2022**, *49* (4), 1−12.

(64) Borjigin, T.; Shen, B. J.; Yu, L. J.; Yang, Y. F.; Zhang, W. T.; Tao, C.; Xi, B. B.; Zhang, Q. Z.; Bao, F.; Qiu, J. Z. Mechanisms of shale gas generation and accumulation in the Ordovician Wufeng−Longmaxi Formation, Sichuan Basin, SW China. *Petrol. Explor. Dev.* **2017**, *44* (1), 69−78.

(65) Tang, X. L.; Jiang, Z. X.; Huang, H. X.; Jiang, S.; Yang, L.; Xiong, F. Y.; Chen, L.; Feng, J. Lithofacies characteristics and its effect on gas storage of the Silurian Longmaxi marine shale in the southeast Sichuan Basin, China. *J. Nat. Gas Sci. Eng.* **2016**, *28*, 338−346.

(66) Loucks, R. G.; Reed, R. M.; Ruppel, S. C.; Hammes, U. Spectrum of pore types and networks in mudrocks and a descriptive

classification for matrix-related mudrock pores. *AAPG Bull.* **2012**, *96* (6), 1071−1098.

(67) Löhr, S. C.; Baruch, E. T.; Hall, P. A.; Kennedy, M. J. Is organic pore development in gas shales influenced by the primary porosity and structure of thermally immature organic matter? *Org. Geochem.* **2015**, *87*, 119−132.

(68) Caillet, G. The caprock of the Snorre Field, Norway: a possible leakage by hydraulic fracturing. *Mar. Petrol. Geol.* **1993**, *10* (1), 42−50.

(69) Liu, S. G.; Jiao, K.; Zhang, J. C.; Ye, Y. H.; Xie, G. L.; Deng, B.; Ran, B.; Li, Z. W.; Wu, J.; Li, J. X.; Liu, W. P.; Luo, C. Research progress on the pore characteristics of deep shale gas reservoirs: An example from the Lower Paleozoic marine shale in the Sichuan Basin. *Natur. Gas Indus* **2021**, *41* (1), 29−41.